

## Viscous flow lobes in central Taylor Valley, Antarctica: Origin as remnant buried glacial ice

Kate M. Swanger<sup>a,\*</sup>, David R. Marchant<sup>a</sup>, Douglas E. Kowalewski<sup>a,1</sup>, James W. Head III<sup>b</sup>

<sup>a</sup> Department of Earth Sciences, Boston University, 675 Commonwealth Avenue, Boston, MA 02215, USA

<sup>b</sup> Department of Geological Sciences, Brown University, 324 Brook Street, Box 1846, Providence, RI 02912, USA

### ARTICLE INFO

#### Article history:

Received 6 October 2009

Received in revised form 11 March 2010

Accepted 21 March 2010

Available online 27 March 2010

#### Keywords:

Periglacial geomorphology

Quaternary

McMurdo Dry Valleys

Ice-cored moraine

Shallow seismic survey

Rock glacier

### ABSTRACT

Viscous flow lobes are common throughout the McMurdo Dry Valleys (MDV) of Antarctica. These features have been described as rock glaciers, gelifluction lobes, solifluction lobes, talus mobilized by pore ice and/or segregation ice, and debris-covered glaciers. We investigate the origin, modification, and flow of a 2-km-long lobe (East Stocking Lobe or ESL) along the north wall of central Taylor Valley using field mapping techniques, shallow seismic surveys, time-dependent displacement surveys, and isotopic analyses of buried-ice samples. On the basis of these integrated analyses, we show that the ESL is cored with remnant glacier ice, most probably derived from an advance of nearby Stocking Glacier ~ 130 kyr BP. Seismic data, coupled with results from ice-flow modeling assuming plastic flow of clean ice, suggest that the buried core of glacier ice is ~ 14- to 30-m thick. Near its terminus, the ESL flows at a rate of ~ 2.4 to 6.7 mm a<sup>-1</sup>. The loose drift that caps the buried ice (typically < 1 m thick) is composed of moderately stratified sand- and gravel-sized clasts; it is dry (1–3% soil gravimetric water content; GWC), except near ephemeral stream channels and the margins of melting snow banks (6–25% GWC). Stable isotopic analyses of samples from the upper 30 cm of the ice lie on a slope of ~ 5.8 (when plotted on a  $\delta D$  vs.  $\delta^{18}O$  graph), well below the local meteoric water line of 7.75, suggesting modification by freeze/thaw processes and evaporation/sublimation. Measured air and soil temperatures show that intermittent melting is most likely possible during summer months where buried ice is  $\leq 35$  cm below the ground surface. Morphological comparisons with ice-cored deposits in upland regions of the Dry Valleys, e.g., Mullins and Beacon Valleys (30 km inland and ~ 500 m higher in elevation), and near the coast (40 km distant and ~ 500 m lower) reveal marked contrasts in the style of near-surface ice degradation and cryoturbation. From these morphological comparisons, we infer that buried-ice deposits in the stable upland zone have not experienced the relatively warm climate conditions now found at the ESL and at lower elevations in the Dry Valleys region (e.g. sustained summertime temperatures of  $\geq -4$  °C) for the last several million years.

© 2010 Elsevier B.V. All rights reserved.

### 1. Introduction

A recent theme in geomorphological research is to understand the age, origin, and modification of buried-ice deposits in polar latitudes (Konrad et al., 1999; Cardyn et al., 2007; Lacelle et al., 2007, 2009). In addition to several specific objectives, these studies provide global baseline data regarding thaw degradation and the future of terrestrial ice loss in a warming climate (Humlum, 1998; Steig et al., 1998a,b; Osterkamp and Romanovsky, 1999). In Antarctica, one application of this research has been to understand the climatic significance of debris-covered glaciers, some of which may contain ice (and possibly atmosphere) of late Miocene age (Sugden et al., 1995; Schaefer et al., 2000; Marchant et al., 2002;

Schorghofer, 2005; Kowalewski et al., 2006). A related inquiry, presented here, is to examine buried-ice deposits whose origin and style of degradation is not yet well understood, and whose climatic significance remains a mystery. It is within this framework that we investigate the age, origin, and evolution of large-scale viscous flow lobes of the McMurdo Dry Valleys region (MDV) of Antarctica.

Viscous flow lobes are common geomorphological elements throughout the MDV (e.g., Hassinger and Mayewski, 1983). In several instances, deposits are simultaneously identified as rock glaciers, gelifluction lobes, solifluction lobes, talus mobilized by pore ice and/or segregation ice, or debris-covered glaciers (Nichols, 1968; Hassinger and Mayewski, 1983; Marchant and Denton, 1996; Marchant and Head, 2007). Because each of these proposed origins requires different environmental forcings, and alternate responses to environmental change (Swanger and Marchant, 2007), we undertook a detailed study of one of the largest such lobes: the 2-km long East Stocking Lobe (ESL) situated near Stocking Glacier on the north wall of central Taylor Valley (Figs. 1 and 2). Our results show that this lobe (and those adjacent to it) are 1) cored by relict glacier ice, 2) reflect former glacial advance during marine oxygen isotope stage 5, and

\* Corresponding author. Current address: Geology Department, Colgate University, 13 Oak Drive, Hamilton, NY 13346, USA. Tel.: +1 315 228 7202; fax: +1 315 228 7187. E-mail address: [kswanger@colgate.edu](mailto:kswanger@colgate.edu) (K.M. Swanger).

<sup>1</sup> Current address: Department of Geosciences, University of Massachusetts, 233 Morrill Science Center, Amherst, MA 01003, USA.

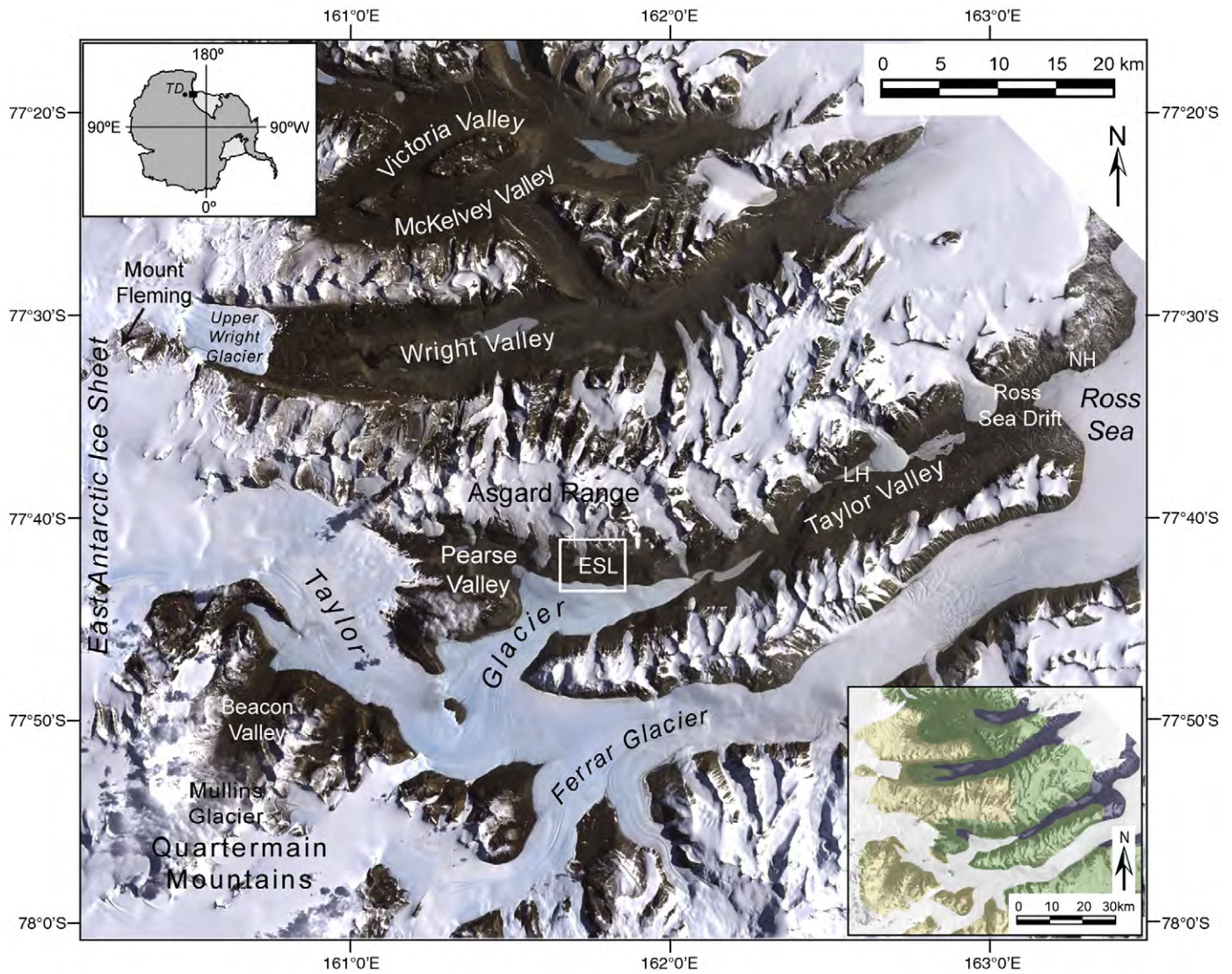


**Fig. 1.** Satellite image of the McMurdo Dry Valleys (MDV), where ESL = east stocking lobe, LH = Lake Hoare, and NH = New Harbour. The study area is shown with a white box. Upper left inset: location map, TD = Taylor Dome. Lower right inset: map of the MDV showing the geographic distribution of the coastal thaw zone (violet/black), inland mixed zone (green/dark grey) and stable upland zone (tan/light grey). Environmental conditions in the coastal thaw zone favor active-layer cryoturbation, solifluction, and thermokarst degradation of buried ice (Denton and Marchant, 2000; Hall and Denton, 2000), whereas those in the upland stable zone foster dry active layers, typically  $\leq 15$  cm thick, preservation of multi-million-year old ashfall deposits, and bedrock erosion rates as low as  $5\text{--}20$  cm  $\text{Myr}^{-1}$  (Sugden et al., 1995; Summerfield et al., 1999; Marchant et al., 2002; Balco and Shuster, 2009). The little-studied (from a geomorphic perspective) inland mixed zone occurs at the transition between these two end member zones (Marchant and Head, 2007).

3) can be used to help constrain local atmospheric warming over the last  $\sim 10^5$  years.

### 1.1. The McMurdo Dry Valleys (MDV)

Located in the central Transantarctic Mountains, the McMurdo Dry Valleys lie between the East Antarctic Ice Sheet (EAIS) and seasonally open water of the Ross Sea (Fig. 1). Local relief is  $\sim 2800$  m. Most regions are generally free of surface ice and there are no vascular plants. Major east–west trending valleys, each  $\sim 80$  km long and up to 15 km wide, extend across the region (Fig. 1).

Meteorological data from automated weather stations show that summer conditions in the MDV vary predictably as a function of increasing elevation and distance from the coast (Doran et al., 2002; Fountain et al., 2009). Given measured variations in summertime atmospheric temperature, soil temperature, soil moisture, and relative humidity, Marchant and Denton (1996) and Marchant and Head (2007)

identified three distinct microclimate zones within the MDV, each with a unique set of endemic landforms. The mapped climate zones include a relatively warm-and-wet coastal thaw zone (CTZ), a cold-and-frozen stable upland zone (SUZ), and a little-studied (from a geomorphological perspective) transitional inland mixed zone (IMZ), in which climate conditions lie between these two end-member zones (Fig. 1 and caption; Table 1). The ESL occurs at the transition between the cold and dry upland landscapes of the MDV (SUZ), and the relatively warm CTZ where young, buried ice of late Wisconsinan age shows abundant evidence for thermokarst and topographic inversion (Denton and Marchant, 2000; Marchant and Head, 2007).

The local bedrock in the MDV consists of a basement complex of Precambrian to Paleozoic age granites and gneisses, most of which were produced and/or deformed during the Cambro-Ordovician Ross Orogeny (Allibone and Wyszczanski, 2002; Giacomini et al., 2007). Inland, at high elevations, these rocks are unconformably overlain by nearly flat-lying sedimentary rocks of the Beacon Supergroup (Devonian to Triassic age

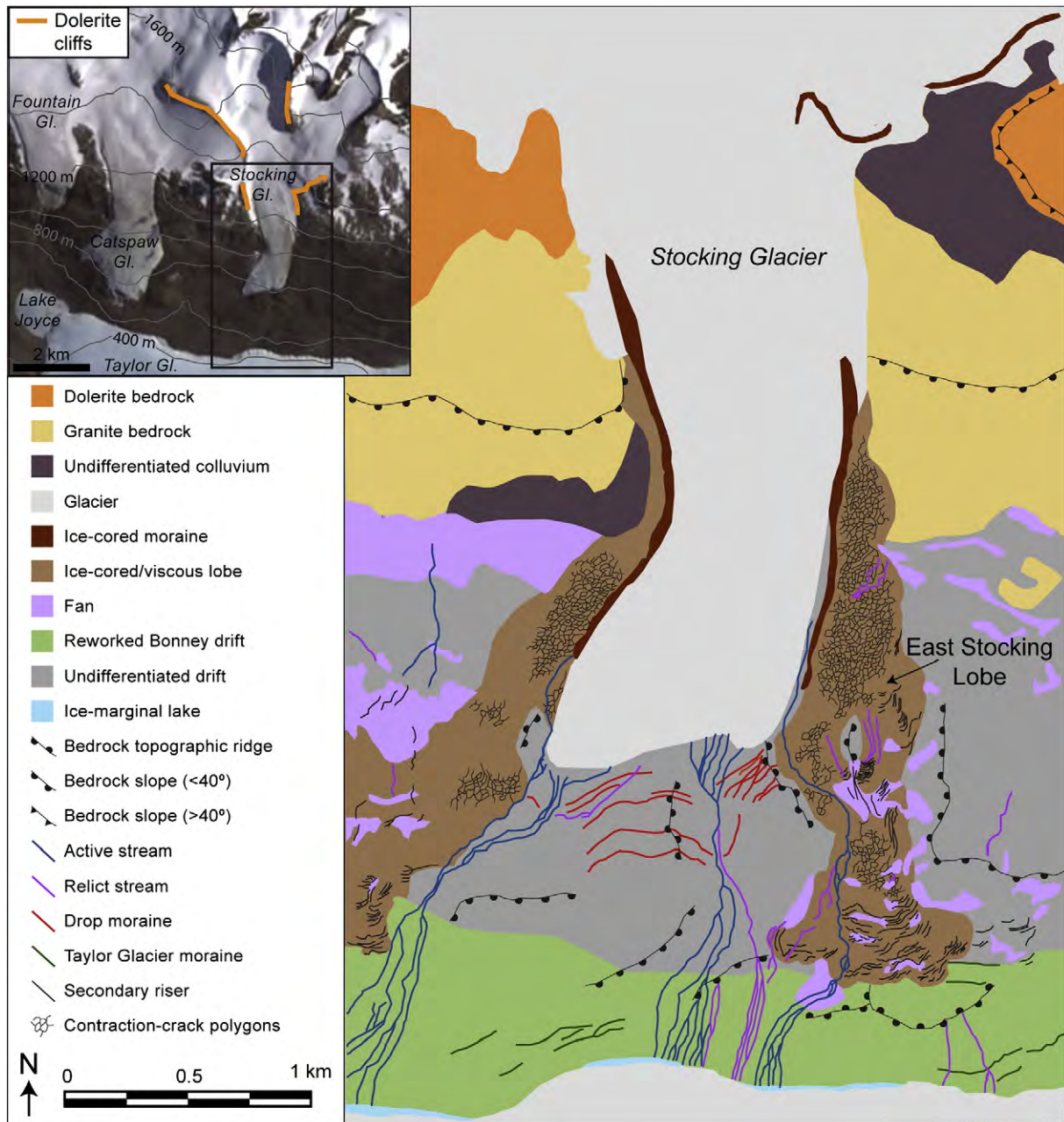


**Fig. 2.** Geomorphic map of features at and near Stocking Glacier. Upper left inset: aerial photograph showing regional location of Stocking Glacier, 200-m contour interval. The black rectangle highlights the region covered in the geomorphic map and the thick orange/black lines highlight dolerite cliffs, from which rockfall is derived, that line the lateral margins of Stocking Glacier. In the foreground, Bonney drift represents the last major advance of Taylor Glacier during marine oxygen isotope stage 5 (MIS 5) (e.g., Higgins et al., 2000; see also Bockheim et al., 2008).

sandstones, siltstones, and conglomerates) (Barrett, 1981). Thick intrusive sills of Jurassic-age Ferrar Dolerite intrude all of these rocks (Elliot and Fleming, 2004).

## 2. Methods and results

Our results are based on a combination of field mapping, shallow seismic surveys, geospatial measurements, isotopic analyses, and numerical flow modeling. As baseline data for our environmental reconstructions, we also measured summertime atmospheric and soil temperature/moisture conditions at several locations throughout the Dry Valleys region (see below and Table 1). We begin with a brief overview of the physical setting of the Stocking Glacier, a small alpine

glacier in central Taylor Valley that occurs proximal to the East Stocking Lobe (ESL) (Figs. 1 and 2).

### 2.1. The Stocking Glacier

The Stocking Glacier lies at the upper elevation limit of the inland mixed zone (IMZ) (Fig. 1 inset). The glacier originates from snow-capped mountains at ~1800 m along the north wall of Taylor Valley, passes through a narrow bedrock constriction with exposed cliffs of Ferrar Dolerite at ~1400–1200 m elevation, and terminates at ~800 m elevation; its equilibrium line rests at ~1250 m elevation (Fountain et al., 1999). Apart from the spatially restricted cliffs of Ferrar Dolerite (Fig. 2), the local bedrock is dominated by smooth, low-angle slopes of weathered granite and gneiss. Stocking Glacier is relatively free of debris,

**Table 1**  
Annual and peak atmospheric and soil conditions from different microclimate zones in the McMurdo Dry Valleys.

	Beacon Valley <sup>a</sup>	East Stacking Lobe <sup>b</sup>	Lake Hoare <sup>c</sup>
Elevation (masl) <sup>d</sup>	1220	610	72
Distance from coast (km)	80	42	15
Mean annual air temp (°C) <sup>e</sup>	−21.9°	−20°	−19.0°
Mean annual soil surface temp (°C) <sup>e</sup>	−21.6°	−20°	−18.8°
Mean annual soil temp at 10-cm depth (°C) <sup>e</sup>	−21.5°	−20°	−18.3°
Mean December air temp (°C) <sup>f</sup>	−8.9°	−3.8°	−3.9°
Mean December soil surface temp (°C) <sup>f</sup>	−3.0°	+3.7°	+6.2°
Mean December soil temp at 10-cm depth (°C) <sup>f</sup>	−5.0°	+1.5°	+2.2°
Mean December air relative humidity (%) <sup>f</sup>	45%	42%	60%
Positive degree-days in summer 2006–2007 <sup>g</sup>	9	51	122
Maximum depth temp >0°C <sup>f</sup>	10 cm	37 cm	n/a
Active layer depth <sup>h</sup>	10 cm (dry)	40 cm (dry)	50–60 cm (wet)

<sup>a</sup> Data for 2006 from the central Beacon Valley meteorological station at the terminus of debris-covered Mullins Glacier.

<sup>b</sup> Data from a meteorological station ~100 m distal to ESL from 12 November 2006 to 3 January 2007. Because of field logistics, data could not be collected during the entire year, and mean annual conditions were based on conditions at the meteorological station in the Pearce Valley (15 km to the west).

<sup>c</sup> Data for 2006 from Long-term Ecological Research website ([http://www.mcmlter.org/data\\_home.htm](http://www.mcmlter.org/data_home.htm)).

<sup>d</sup> Meters above sea level.

<sup>e</sup> From 1 January 2006 to 31 December 2006.

<sup>f</sup> For 1 December to 31 December 2006.

<sup>g</sup> Positive degree-days (PDD) are computed for the austral summer of 2006–2007 (1 October 2006 to 1 March 2007) using 0 °C as a minimum threshold:

$$PDD = \left( \frac{T_{Max} + T_{Min}}{2} \right) - T_{Base}$$

where  $T_{Max}$  = maximum daily temperature if >0 °C,  $T_{Min}$  = minimum daily temperature if >0 °C,  $T_{Base}$  = 0 °C. Data for east stocking lobe come from our long-term meteorological station from Pearce Valley (~15 km west of ESL at ~400 m elevation) and data for Lake Hoare are from our New Harbour station (~15 km to the east at ~20 m elevation) (see Fig. 1 for locations).

<sup>h</sup> Maximum depth at which measured soil temperatures were >0 °C. Dry indicates that gravimetric water content (GWC) of soil >0 °C is <3%, wet indicates GWC>3%.

except for scattered englacial and supraglacial clasts that are concentrated at lateral ice margins forming the modern ice-cored moraines (Fig. 2; see also Discussion).

Small meltwater streams occur on the surface of Stacking Glacier, typically originating where dolerite debris on the glacier surface is heated by solar radiation to temperatures >0 °C. These streams flow along the lateral margins of the glacier and have deposited stratified sands and fine gravels (granite grus and disaggregated mineral grains from Ferrar Dolerite). Meltwater streams eventually extend outward from the glacier and flow down the north wall of Taylor Valley, cutting small channels in unconsolidated debris (e.g., Atkins and Dickinson, 2007), including debris that caps the ESL (Fig. 2).

Ice-cored moraines from Stacking Glacier are restricted to lateral-ice margins; they do not occur at the glacier front (Fig. 2). The likely explanation for this unusual pattern comes from the highly localized distribution of rockfall onto the surface of Stacking Glacier. Rock fall production is essentially restricted to locations with dolerite cliffs, which today occur only alongside lateral-ice margins in a few places between 1200 and 1400 m elevation, not at the head of Stacking Glacier (Fig. 2). This distribution concentrates debris at lateral-ice margins, but not at the glacier snout, and gives rise to two distinct types of ice-marginal deposits: high-relief, ice-cored moraines along the lateral margins (with extensive supraglacial debris, sometimes stratified) and isolated drop moraines (parallel lines of stacked clasts arrayed in ridges 1–2 cobbles high and devoid of intervening ice) at the glacier snout. The latter are formed by intermittent release of scattered dolerite cobbles along a stationary ice front (Fig. 2). Because Stacking Glacier is almost certainly cold-based (none of the clasts transported by Stacking Glacier contain evidence for glacial abrasion, e.g., striations, molding, polish, and faceting), basal regelation is not a viable mechanism for significant debris entrainment (Cuffey et al., 2000).

## 2.2. The morphology of the East Stacking Lobe

The East Stacking Lobe (ESL) originates alongside the eastern margin of Stacking Glacier, at about 1200 m elevation, and extends ~2 km down the north wall of Taylor Valley (Figs. 2 and 3). Over this distance, the ESL descends ~600 m and displays several notable changes in surface morphology. At its head, the ESL occupies a shallow depression

adjacent to Stacking Glacier. Here, its surface dips downslope at about 5–8° and is marked with a network of interlocking, randomly oriented contraction-crack polygons (Figs. 2–4). At ~850 m elevation, the slope of the ESL increases abruptly to ~20° and the polygons give way to lobate steps and compressional ridges suggestive of differential flow (Figs. 3 and 4A). At ~800 m, the ESL wraps around the base of an upstanding bedrock knob and, for a short distance, forms two distinct sublobes, each with numerous steps and ridges (Figs. 3 and 4A). Thereafter, the sublobes converge, the slope angle of the ESL returns to ~5–8°; and its surface topography is again dominated by numerous, randomly oriented contraction-crack polygons. At ~650 m elevation the ESL terminates abruptly, forming a broad, multicuspate arc, ~1 km wide, that rises ~30 m above surrounding terrain (Figs. 3 and 4B).

Several stream channels extend from Stacking Glacier and cut across the ESL (Figs. 2 and 4). The longest stream dissects the western portion of the ESL, eroding a narrow V-shaped channel as much as 2 m deep (Figs. 2 and 4). This channel bifurcates, forming a narrow braided network where slope angles decrease to ≤8°, as occurs about halfway down the ESL (in the zone of contraction-crack polygons, Figs. 3, 4 and 5G). Sediment transport within stream channels is sporadic. Fans of stratified debris form at breaks in channel gradients and at the terminus of most large-scale sublobes and ridges (Figs. 2 and 4). Where windblown snow accumulates in these channels, melting snow may contribute a significant fraction of the total discharge during early summer months (e.g., Head et al., 2007; Levy et al., 2008).

The detailed morphology of stream channels and fans enables classification of both modern and relict stream systems. Modern stream systems show well-defined channels and pristine fans; whereas relict streams typically display subdued channel walls and dissected fans with various stages of winnowing, wind transport (formation of surface ripples), and deflation (formation of weak desert pavements) (Fig. 4).

At the small scale, the surface of the ESL (apart from fan deposits) exhibits weathered boulders and cobbles of dolerite (~50%), granite (~40%), and gneiss/schist (~10%), with intervening granite grus. On average, boulder density is 1–3 boulders/m<sup>2</sup>. Ventifacts (rocks that have been abraded, polished, and/or shaped by saltating sands) occur (e.g., Gillies et al., 2009) but are uncommon and typically restricted to dolerite clasts with mineral grains <~2 mm in diameter.

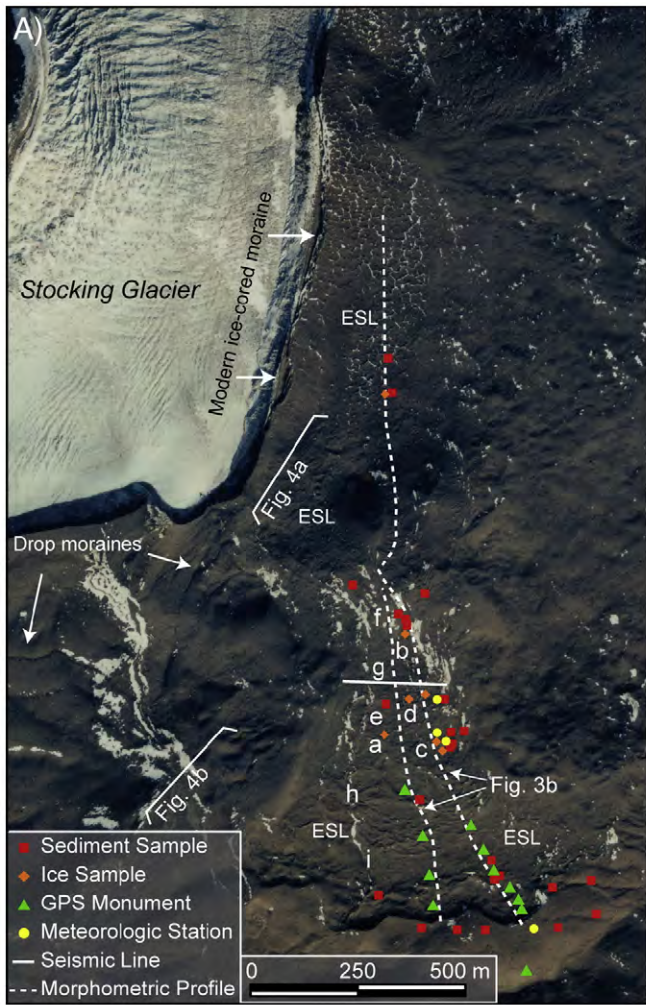


**Fig. 3.** (A) Vertical aerial photograph showing the lower portion of the ESL (center) and drop moraines beyond the terminus of the Stocking Glacier centerline. Locations for Figs. 4A and B are shown as numbered brackets that open in the direction of view. Letters a–i indicate the locations of photographs in Fig. 5. (B) Morphometric profiles for the ESL (locations plotted in Fig. 3A). The dashed portion of the east transect is inferred from topographic maps and not measured directly in the field. The location of GPS monuments, prominent ridges, and contraction-crack polygons are also plotted; the polygons only occur on slopes of  $<8^\circ$ , whereas compressional ridges characterize most higher angle slopes. GPS monuments are shown as numbered arrows.

### 2.3. Meteorological and soil-environmental conditions at the study site

To determine the range of summertime atmospheric and soil-environmental conditions along the ESL, we installed a suite of HOBO™ SmartSensor data loggers (Onset Computer Corporation, Inc.) at four localities (all between 600 and 1000 m elevation; Fig. 3) during the

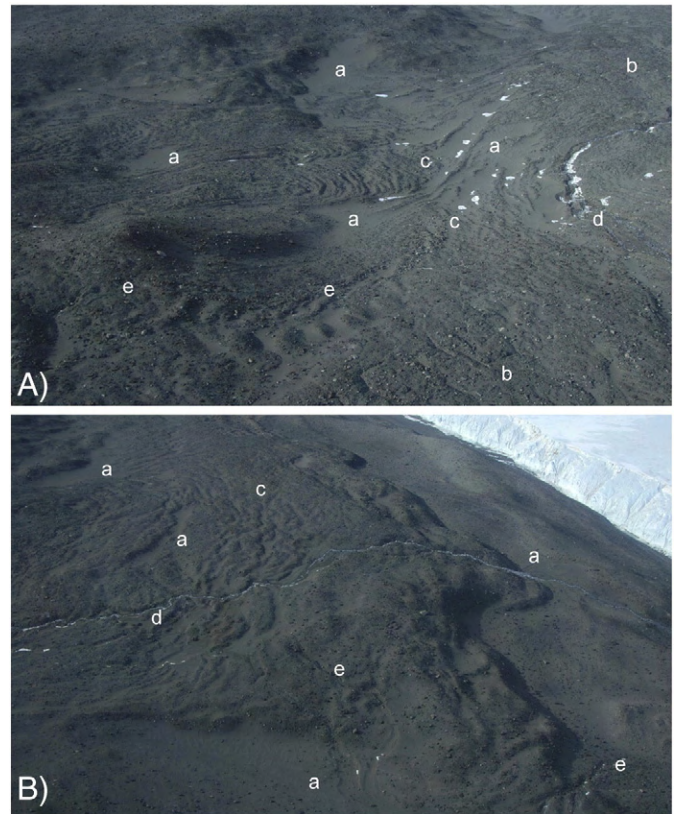


**Fig. 4.** (A) Oblique aerial photograph of the upper portion of the ESL, view to the SE (see Fig. 3A for location) in which a = fan, b = contraction-crack polygons, c = compressional ridges, d = active stream, and e = relict stream. From right to left, the photograph shows: ice-cored drift adjacent to Stocking Glacier, divergent flow around a bedrock topographic high, relict stream channels and fans, and gentle slopes that feature contraction-crack polygons. The width of the photograph in the foreground is  $\sim 300$  m. (B) Oblique aerial photograph of the terminus of the ESL, view to the southeast (location in Fig. 3A). There are numerous compressional ridges and steps that lie parallel with the main, arcuate front of the lobe. Also shown are relict and active streams and scattered fans. The lobe terminus rises  $\sim 30$  m above the surrounding wall of Taylor Valley and is cut, in one location, by an active stream channel. Width of the photograph in the foreground is  $\sim 300$  m.

austral summers of 2004/5 and 2006/7 (Table 1). At each site, we measured air temperature and relative humidity (both at 10 cm above the ground surface) and soil temperatures at 0 cm (ground surface) and subsequent 10-cm depth increments (down to at least 40-cm depth or to the top of buried ice, see below). We also measured soil-moisture conditions at multiple depths, with most probes within 10 cm of the ground surface and some resting directly on top of buried ice at  $\sim 35$ -cm depth (Fig. 3).

The full results of our meteorological survey, including data from other, nearby locations in the MDV, are presented in Table 1. The maximum recorded atmospheric temperature at the ESL was  $3.4^\circ\text{C}$ ; this yielded the highest soil-surface temperature of  $11^\circ\text{C}$  and the maximum penetration of the  $0^\circ\text{C}$  soil isotherm to  $\sim 37$  cm (Table 1).

### 2.4. The sedimentology of debris capping the East Stacking Lobe

Loose, unconsolidated, and bedded sands dominate the uppermost 30+ cm of the ESL (Table 2). Most commonly, the debris shows alternating layers (1–5 cm thick) of medium- to coarse-grained sand and fine-grained gravel; cross beds are planar and typically restricted to horizons with medium sand-sized grains. In places, subangular to subrounded clasts of dolerite ( $\sim 50\%$ ), granite ( $\sim 40\%$ ), and schists/gneisses ( $\sim 10\%$ ) occur sporadically throughout the deposit (percentages match average values for these lithologies exposed as cobbles at the surface of the modern ice-cored moraines). None of these clasts

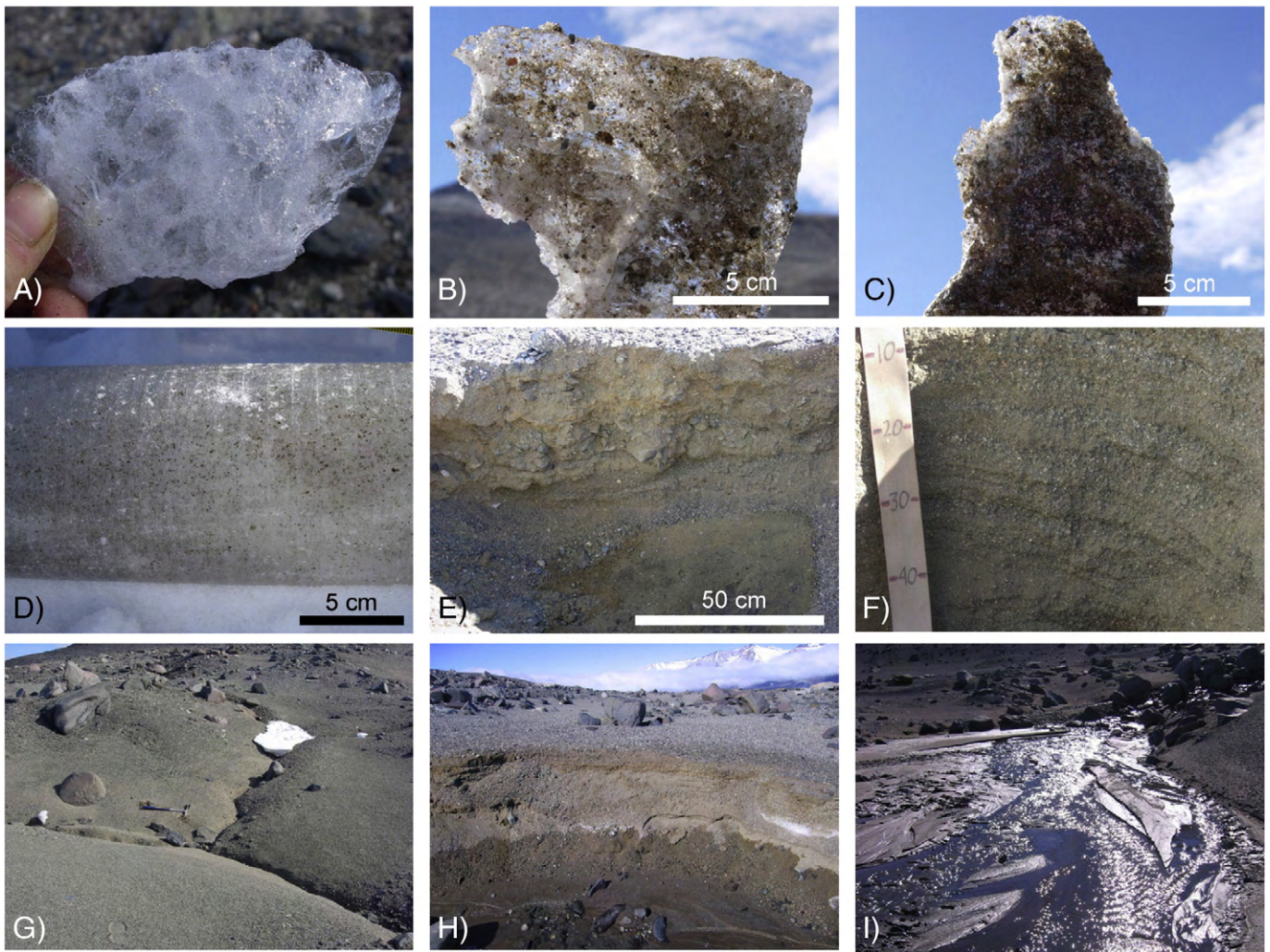


**Fig. 5.** Mosaic of features associated with the ESL; locations for each panel are shown in Fig. 3A. (A) clean, bubbly ice (excess ice) encountered at several localities; (B), an example of excess ice containing ~5–10% dispersed debris; (C) pore ice with a GWC of ~26%; (D) a section of an ice core (~10-cm diameter) recovered from the ESL at the seismic-survey site. The debris content, which falls between values shown in (A) and (B) is constant throughout the 1.8-m long core. (E) and (F) are stratified and reworked drift exposed in hand-dug soil pits within the ESL; the moderately sorted and stratified sand-and-gravel layers in (F) are from a relict fan deposit. (G) contraction-crack polygons that mark the surface of gentle gradients on the ESL (ice pick for scale). (H) Cut bank and gravel-covered channel floor of the main stream dissecting the ESL; note wicking of water in sediments along the cut bank and the presence of salt precipitates (white layer along right edge of the photograph); width of photograph is ~1 m. (I) Oblique view of the main meltwater stream where slope decreases and the channel bifurcates. Field of view in foreground is ~1.5 m.

show evidence for glacial modification (e.g. striations, polish, and molded facets). The bedded matrix fraction is made up of disaggregated mineral grains from Ferrar Dolerite (principally pyroxene and plagioclase) and granite grus. Apart from regions along the margins of isolated snow banks and ephemeral streams, the bedded sediments are very dry. Analyses of soil gravimetric water content (GWC) indicates <1% moisture by weight. Alongside stream channels and scattered snow banks, however, surface sediments are visibly moist and contain from 1 to >5% GWC (e.g., Northcutt et al., 2009). The abundant evidence for bedded and stratified sediments throughout the ESL points toward considerable reworking by liquid water (e.g. Bennett et al., 2000; Moorman and Michel, 2000).

### 2.5. Observed ice deposits within the East Stocking Lobe

Shallow, hand-dug excavations in the ESL reveal the presence of pore ice and excess ice (the latter is ice that exceeds available pore space). Pore ice is typically found between 10 and 20 cm depth alongside local meltwater sources, including the margins of melting snow banks and/or ephemeral streams. The gravimetric water content of pore ice ranges between 6 and 25% (~10 to 40% volumetric water content if thawed).

Such pore ice is locally common all along the north wall of central Taylor Valley and does not appear to be a unique attribute of the ESL. The surface of excess ice typically occurs below pore ice (if present) and at depths approaching 1–2 m (although it may be as shallow as ~35 cm; Table 3). Excess ice in central Taylor Valley is rare and appears to be a unique attribute of the ESL and of similar appearing viscous lobes in the region (e.g., Hassinger and Mayewski, 1983). In most locations, the surface of excess ice is smooth, planar, and dry, even during summer months (Fig. 5E).

Detailed examination of the surface of excess ice (e.g., the ice table) reveals some spatial variation in debris content, with estimated values ranging from <5% debris in regions with relatively clean ice, to as much as 50% debris in sandy ice (Fig. 5A–B). The sands are typically oriented in near-vertical veins and wedges that cut the ice and most likely reflect the development and partial infill of thermal contraction cracks (e.g., Berg and Black, 1966; Marchant et al., 2002). Shallow ice cores suggest that the observed concentration of debris at the ice surface at any one locality faithfully represents the concentrations at depth; e.g., at the two locations cored, there were no marked variations in debris content within the uppermost 2 m of excess ice; at both sites, values averaged ≤5% debris by volume (Fig. 5D).

**Table 2**  
Sedimentology of ESL drift.

Sample <sup>a</sup>	Grain size <sup>b</sup>	Graphic mean grain size ( $\phi$ ) <sup>c</sup>	Inclusive graphic standard deviation ( $\phi$ ) <sup>d,e</sup>
04-42a	5:92:3	1.5	1.4
04-42b	11:87:2	1.2	1.5
04-44	21:73:6	1	2.2
04-47b	14:78:8	1.3	1.8
04-51	19:76:5	1	2.1
04-57	16:83:1	1.2	2
04-58	26:70:4	0.8	1.8
04-59	14:84:2	0.7	1.3
04-60a	21:75:4	0.8	2
04-65	18:76:6	1.2	1.9
04-67	13:82:5	1.3	1.9

<sup>a</sup> Sediment samples were analyzed for grain-size and lithology; these were dry-sieved in the field, and the 16- to 64- mm fraction was examined for evidence of glacial abrasion (striations, polish, molding) and lithologic constituents (dolerite, gneiss, and granite). The <16-mm fraction was analyzed at Boston University using standard wet and dry sieving procedures in order to calculate the relative weight percent of fine gravel, sand, silt, and clay.

<sup>b</sup> Ratio of gravel : sand : mud in the <16-mm fraction.

<sup>c</sup> Graphic mean grain size:  $M = \left( \frac{\phi_{16} + \phi_{50} + \phi_{84}}{3} \right)$  where  $\phi$  is the  $\phi$  size of the xth percentile.

<sup>d</sup> Inclusive graphic standard deviation:  $M_2 = \left( \frac{\phi_{84} - \phi_{16}}{4} \right) + \left( \frac{\phi_{95} + \phi_5}{6.6} \right)$  where  $\phi_x$  is the  $\phi$  size of the xth percentile.

<sup>e</sup> Graphic standard deviation is determined for bulk sediment samples and, thus, includes interbedded sands and fine gravels. Although these data indicate poorly sorted sediments, individual beds/laminations are moderately sorted.

### 2.5.1. Isotopic composition of measured excess ice

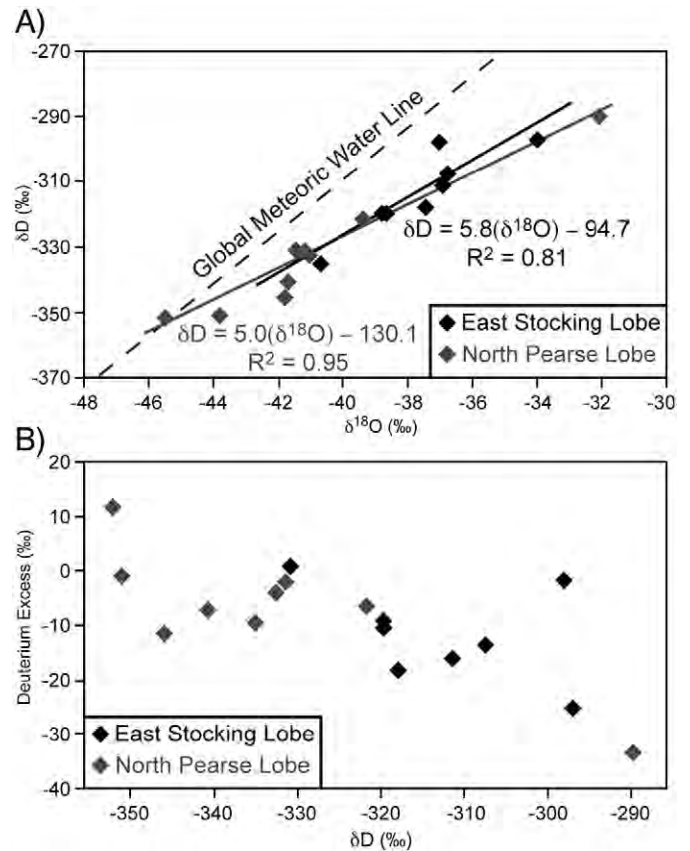
Ice samples for  $\delta^{18}\text{O}$  and  $\delta\text{D}$  analyses were collected from 10 to 30 cm below the ice table, double-bagged in Whirl-Pak bags, and kept frozen at  $-20^\circ\text{C}$  until analyzed. Analyses were conducted on an isotope ratio mass spectrometer at the Boston University Stable Isotope Laboratory (see specifications in Fig. 6 caption).

Fig. 6 displays results from eight samples of excess ice (site locations plotted in Fig. 3). When plotted on a graph of  $\delta^{18}\text{O}$  vs.  $\delta\text{D}$ , the results fall below the global and local meteoric water lines (GMWL and LMWL) of  $\sim 8$  and  $\sim 7.75$ , respectively (Craig, 1961; Gooseff et al., 2006), with the best-fit line yielding  $\delta\text{D} = 5.8 \times \delta^{18}\text{O} - 94.7$  ( $R^2 = 0.81$ ; Fig. 6). Deuterium excess values are negative, ranging from  $-1.9\%$  to  $-25.2\%$ , with an average value of  $-13.1\%$ . Fig. 6 also shows  $\delta^{18}\text{O}$  vs.  $\delta\text{D}$  data for excess ice in similar ice-cored viscous lobes in nearby Pearse Valley (Fig. 1). As detailed in Figs. 6 and 7 (and captions), the results suggest that at least the upper  $\sim 30$  cm of the ice has been modified by melting and refreezing, accompanied by sublimation and/or evaporation.

**Table 3**  
Depth to ice within ESL.

Sample	Depth to ice/ice cement <sup>a</sup>
04-53	25 cm (IC)
04-54	50 cm
04-55	30 cm (IC)
04-56	25 cm (IC)
04-57	27 cm (IC)
04-58	44 cm
04-59	60 cm (IC)
04-60	35 cm
04-66	45 cm
04-67	40 cm
04-69	35 cm
06-07	40 cm
06-08	60 cm
06-09	40 cm
06-10	35 cm

<sup>a</sup> Denotes depth to ice in the ESL. The ice is excess ice unless noted as IC, in which case the measurement is to the buried surface or pore ice (ice cement). All samples come from the region with contraction-crack polygons in the central portion of the ESL (see Figs. 3 and 5).



**Fig. 6.** (A) Plot of  $\delta\text{D}$  vs.  $\delta^{18}\text{O}$  from ice samples within the upper 10–30 cm of excess ice in the ESL (and an ice-cored lobe in Pearse Valley located  $\sim 15$  km west of the ESL) (Fig. 1). Together, the samples fall on a slope of  $\delta\text{D} = 5.3 \times \delta^{18}\text{O} - 115.1$ ,  $R^2 = 0.93$ . (B) Plot of deuterium excess vs.  $\delta\text{D}$  for samples plotted in (A). The very negative deuterium excess values and the slope of 5.3 indicate that the ice has probably been affected by melting and refreezing coupled with evaporation/sublimation (Souchez and Lorrain, 2006). Analyses for  $\delta^{18}\text{O}$  were done via  $\text{CO}_2$  equilibration; deuterium analyses were done via pyrolysis using a GVI ChromeHD™ system. Analytical precision for both typically is  $\pm 0.1\%$ . Isotope values are presented as per mil (‰) relative to VSMOW. Deuterium excess (d) values were calculated as  $d = \delta\text{D} - 8\delta^{18}\text{O}$  after Dansgaard (1964).

### 2.6. Seismic analyses and inferred thicknesses of excess ice in the East Stacking Lobe

To determine the thickness of excess ice in the ESL, we conducted a shallow seismic refraction survey using a Geometrics Geode seismograph with 12 geophones (40 Hz). All data were recorded on a laptop running the Geometrics acquisition software (see details in Figs. 2 and 8). We used a 5-m spacing interval for geophones, a sampling interval of 0.031 ms, and a recording length of 0.2 s. All 12 geophones were imbedded directly into buried ice after removing overlying dry debris. A 5.45-kg (12-lb) sledgehammer struck on an aluminum plate on the buried-ice surface served as the seismic source. We employed a source-moveout survey design, with a stationary geophone array and a moving source. For each source offset, we conducted 6–10 stacks of 10 shots each. All seismic data were analyzed with the open source SeisUnix software package developed at the Center for Wave Phenomena at the Colorado School of Mines (Stockwell, 1999). Figs. 3 and 8 show the location of the seismic survey line.

For both the forward and reverse lines (Figs. 3 and 8), the direct wave traveled at  $\sim 3700 \text{ m s}^{-1}$ , consistent with previous seismic studies on viscous-flow features cored with relatively clean ice in the MDV (e.g., P-wave velocities ( $V_p$ ) of  $3500\text{--}4200 \text{ m s}^{-1}$  from Hassinger and Mayewski, 1983; Shean et al., 2007; Shean and Marchant, 2010). On the reverse line, the refracted wave had a  $V_p = 5500 \text{ m s}^{-1}$ , characteristic of

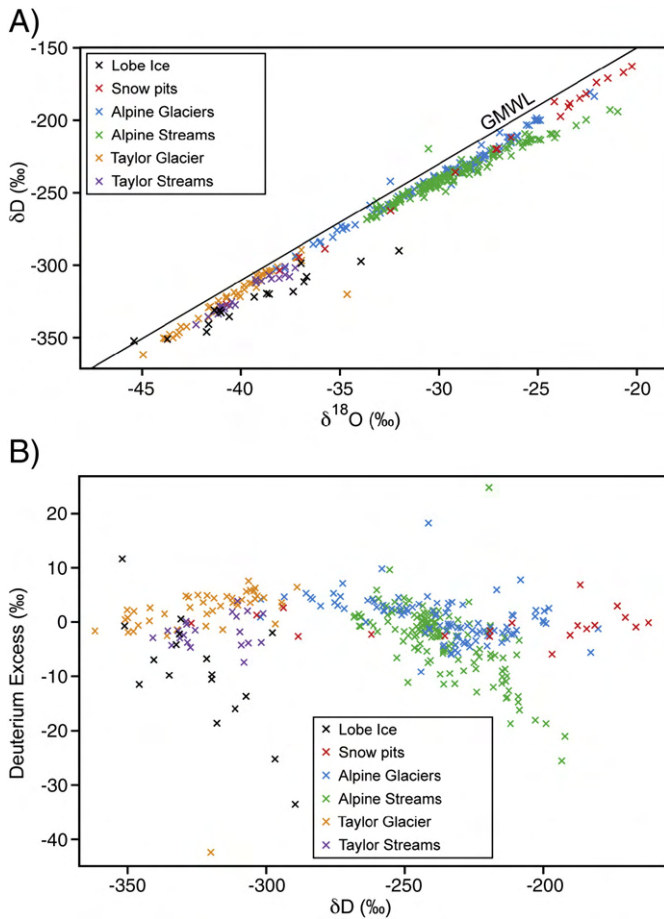


**Fig. 7.** (A) Comparison of isotopic values for ice, water, and snow in Taylor Valley, including ice from the ESL, Pearse Valley, Taylor Glacier, and alpine glaciers nearer to the coast (i.e. east of the ESL). Data also include stream water sourced from these alpine glaciers and from Taylor Glacier, as well as fresh snowfall from the surface of coastal alpine glaciers in Taylor Valley. All data except subsurface ice samples are from [Gooseff et al. \(2006\)](#). Best-fit lines fall on slopes of 7.75 for alpine glaciers and Taylor Glacier, 6.0 for meltwater streams from alpine glaciers, and 5.3 for the subsurface ice in the lobes examined here. [Gooseff et al. \(2006\)](#) surmised that significant evaporation fractionation in stream channels caused the  $\delta D$  vs.  $\delta^{18}O$  of the water to fall well below the global meteoric water line. Similarly, we surmise that stable isotopes from subsurface ice in the ESL fall below the meteoric slope of  $\sim 8$  (instead plotting on a slope of 5.3) due to melting and refreezing and/or evaporation/sublimation. GMWL = global meteoric water line. (B) Plot of deuterium excess vs.  $\delta D$  for all Taylor Valley samples. The sampled glaciers in Taylor Valley have an average deuterium excess of 0.75‰. The average deuterium excess of buried ice in the ESL and in Pearse Valley is  $-9.2\%$ . Only meltwater affected by evaporation in Taylor Valley exhibits such negative deuterium excess values (e.g., [Gooseff et al., 2006](#); [Souchez and Lorrain, 2006](#)).

the seismic velocity for igneous and metamorphic bedrock ([Hassinger and Mayewski, 1983](#)) and fully consistent with the local bedrock geology.

Assuming a simple two-layer model of ice and underlying bedrock, the seismic results at this site suggest a layer of excess ice  $\sim 13.8$  m thick that extends a minimum of 150 m in an east–west direction (the length of the seismic line); the ice most probably rests directly on igneous/metamorphic bedrock ( $V_p = 5500 \text{ m s}^{-1}$ ) ([Fig. 8](#)).

### 2.7. GPS surveys and calculating rates of horizontal flow for the ESL

To determine horizontal flow velocities for the ESL, we installed 10 GPS monuments in large boulders (each  $> 1 \text{ m}^3$  and imbedded in drift and/or ice) in two transects along lower portions of the ESL ([Fig. 3](#)). Monuments were screwed into rock holes drilled using a hand drill with a 3/4-inch (1.9-cm) diamond-tipped bit. In the absence of exposed bedrock, an immense boulder ( $> 3 \text{ m}^3$ ) located on a flat bench  $\sim 100$  m beyond the terminus of the ESL served as a local base station. The

positions of each monument were referenced to this base station which, in turn, was referenced to a continuously monitored GPS station (UNAVCO) at Mount Fleming (FLM5),  $\sim 45$  km to the northwest ([Fig. 1](#)).

Over the 25-month period (10 December 2004 to 9 January 2007), total horizontal displacements ranged from 5.0 to 13.9 mm, and displacements were typically greatest near the margin of individual sublobes and steps ([Table 4](#)). The base station showed the lowest measured displacement of 1 mm (which is within measurement error), demonstrating the efficacy of this approach and confirming that unconsolidated debris in front of the ESL is stable over the timescales considered here.

Both transects show similar average horizontal displacements of 8–9 mm (e.g., an average displacement rate of  $4\text{--}4.5 \text{ mm a}^{-1}$ ) and average displacement directions from  $156^\circ$  to  $177^\circ$  east of north ([Table 4](#)). A notable result in the displacement data comes from the western transect in which the three monuments nearest the terminus moved between 5.0 and  $7.2 \pm 2.5$  mm, while the most northern (upslope) boulder (located at the toe of a 4-m-high step) moved a considerably greater distance of  $13.9 \pm 2.0$  mm. These data suggest that compressional forces are likely instrumental in producing individual steps and risers on the ESL.

## 3. Discussion

### 3.1. The origin of excess ice in the East Stocking Lobe

On the basis of limited field data, [Marchant and Head \(2007\)](#) identified the ESL as a gelifluction lobe and inferred that internal ice was present but that it most probably formed by the freezing of pore water rather than the burial of glacier ice (as occurs in the coldest, high-elevation regions of the MDV). Supported by the new information presented here, we reexamine this conclusion.

The isotopic data for the excess ice, limited to samples from the uppermost 30 cm of the deposit, are indeed consistent with ice derived as segregation ice, but they are also consistent with a core of glacier ice that has been modified in its uppermost  $\sim 30$  cm by local freeze/thaw and evaporative processes. Factors in favor of a wholly segregation-ice origin include observational, stratigraphic, and isotopic data that call for flowing water, saturated sediments (streams, bedded sands, and fan deposits), and near-surface melting and refreezing. Given these factors, cryosuction (which draws water to a freezing front, e.g., [Mackay, 1972](#); [Cheng, 1983](#)) can, under ideal conditions, produce layers of segregation ice up to 6+ m thick ([Lawson, 1983](#); [Mackay and Dallimore, 1992](#)). However, arguments against the segregation-ice origin come from specific details regarding the local climate and textural characteristics of the ESL. First, the formation of meters-thick layers of segregation ice requires relatively warm climate conditions, with mean annual temperatures above  $-10^\circ\text{C}$ ; these warm conditions are required to sustain liquid water migration throughout much of the year ([Mackay and Dallimore, 1992](#); [Allard et al., 1996](#)). Second, thick segregation ice typically forms only in silt-rich soils, which provide the high capillary pressures required for sustained cryosuction ([Mackay, 1972](#); [Mackay and Dallimore, 1992](#); [Allard et al., 1996](#); [Clark et al., 1998](#); [Konrad, 2005](#)). Third, the modern meltwater streams on the ESL are erosional, cutting into the ice-rich deposit, rather than producing significant quantities of subsurface ice. Fourth, climate and environmental reconstructions suggest that conditions at the ESL have not changed appreciably over the last  $10^5$  to  $10^6$  years ([Petit et al., 1999](#); [Higgins et al., 2000](#)). Altogether, this suggests that the inferred origin of excess ice in the ESL as a thick layer of segregation ice is not valid.

In considering a glacial origin for the excess ice, we examined the morphologic setting and areal distribution of the ESL. We suggest that the ESL represents a relict ice-cored moraine, formed at a time when Stocking Glacier was more extensive than at present, and when the rate of rockfall may have been higher in order to produce more extensive ice-cored deposits than is possible at present (e.g., [Ackert, 1998](#)). As shown

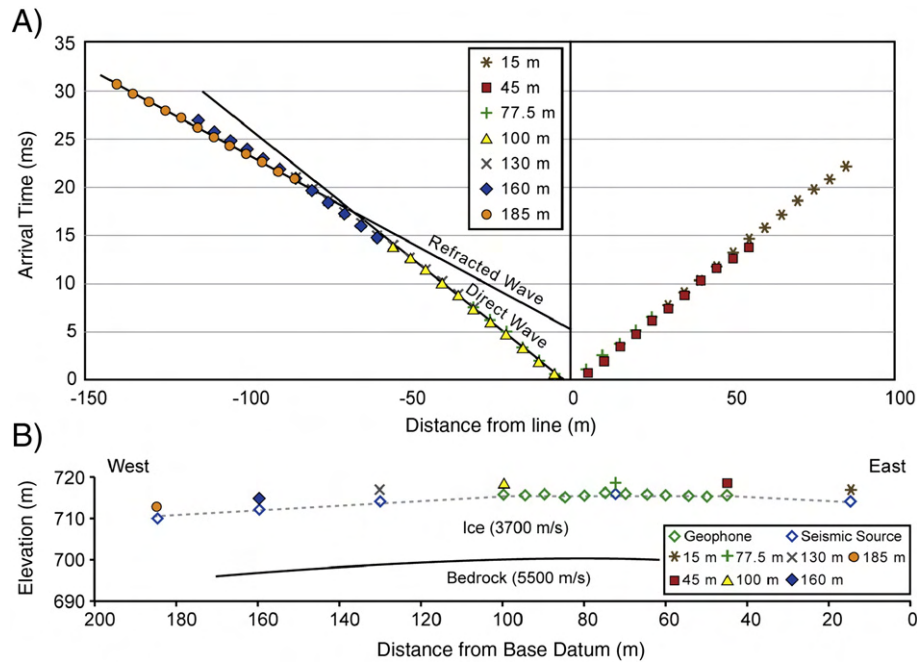


**Fig. 8.** (A) First arrival of  $P$ -wave for the shallow seismic refraction survey (for location see Fig. 3). Results show a direct wave with a  $P$ -wave velocity ( $V_p$ ) of  $3700 \text{ m s}^{-1}$  and a refracted wave of  $V_p = 5500 \text{ m s}^{-1}$ , consistent with  $V_p$  for ice and igneous/metamorphic bedrock, respectively (Hassinger and Mayewski, 1983; Shean et al., 2007; Shean and Marchant, 2010). (B) Cross section for a two-layer solution to the seismic refraction survey. X-axis denotes an arbitrary baseline defined in the field. Open diamonds represent locations of geophones and the seismic sources; symbols above the diamonds correspond to symbols used in (A) to denote the location of each source. The coordinates and elevations for each geophone and source offset were determined using GPS in collaboration with UNAVCO. The moving sledgehammer source was repositioned on the western side of the array at 100, 130, 160, and 185 m (reverse line), on the eastern side of the array at 45 and 15 m (forward line), and at the center of the array at 27.5 m from either end. Assuming the ice–bedrock interface is planar and parallel to the ice surface, the subsurface ice is 13.8 m thick at this location.

in Fig. 2, the ESL originates near, and lies parallel with, modern ice-cored moraines along Stocking Glacier (e.g., Bockheim et al., 2008). We note that a corresponding viscous flow lobe (possibly ice cored) also crops out on the western side of Stocking Glacier, and that the drift on top of the ESL and its correlative western lobe matches the general lithologies and textural characteristics of modern ice-cored moraines alongside Stocking Glacier. Taken together, the data suggest that the ESL is an ice-cored moraine that has flowed a considerable distance downslope, such that it now terminates well beyond the position of maximum ice extent as recorded by drop moraines at the glacier centerline (Fig. 2; see also

Fig. 9 for an alternate explanation for the distribution of ancient ice-cored moraines alongside Stocking Glacier).

### 3.2. Numerical modeling: determining ice thicknesses throughout the East Stocking Lobe

Our seismic results show that the ESL at the survey site contains  $\sim 13.8 \text{ m}$  of relatively clean ice. To determine if the rest of the ESL is similarly cored by ice, we employed the clean-ice-core flow model of Liboutry (1966) as cited in Whalley and Martin (1992) to gauge ice thickness near the terminus and to calculate predicted flow velocities at the shallow seismic survey site:

$$h = \{(n + 1)u / [B(\rho_i g \sin \alpha)]^n\}^{1/n + 1} \quad (1)$$

where  $h$  is the ice thickness,  $n$  is the flow parameter (assumed to be 3),  $u$  is the surface velocity,  $B$  is a temperature-dependent constant,  $\rho_i$  is density of ice,  $g$  is gravitational acceleration, and  $\alpha$  is the slope angle. We calculated  $B$  after Paterson (1994), assuming a mean annual ice temperature of  $-20 \text{ }^\circ\text{C}$  (the local mean annual atmospheric temperature).

For regions near the terminus of the ESL, the results suggest a core of clean ice between 27 and 30 m thick. This calculated thickness is in good agreement with the measured height of the terminus of ESL at  $\sim 30 \text{ m}$  and suggests that a solid core of relatively clean ice lies beneath 1+ m of overlying drift.

Next, assuming i) a clean ice core 13.8 m thick at the seismic survey site, ii) a measured surface slope of  $7^\circ$ , and iii) a mean ice temperature of  $-20 \text{ }^\circ\text{C}$ , we calculated predicted flow velocities at the survey site. If the modeled velocities match the general geomorphology for limited flow, such as randomly-oriented polygons and an absence of surface lobes and steps (see also Whalley and Martin, 1992; Serrano and Lopez-Martinez, 2000; Kaab and Weber, 2004; Levy et al., 2006; Shean et al., 2007), then we would have greater confidence in estimating the thickness of excess ice throughout the ESL. Our modeling results predict a horizontal velocity of as little as  $1\text{--}2 \text{ mm a}^{-1}$ , consistent with geomorphic evidence

**Table 4**  
Displacement distances, rates, and directions measured for GPS monuments on ESL.

GPS monument <sup>a</sup>	Displacement distance (mm) <sup>b</sup>	Displacement rate (mm a <sup>-1</sup> ) <sup>c</sup>	Displacement direction <sup>d</sup>
Base station	<1	n/a	n/a
1	$7.2 \pm 2.3$	3.5	$146^\circ$
2	$5.0 \pm 2.5$	2.4	$180^\circ$
3	$7.1 \pm 2.0$	3.4	$171^\circ$
4	$13.9 \pm 2.0$	6.7	$159^\circ$
5	$7.6 \pm 1.7$	3.7	$157^\circ$
6	$11.7 \pm 1.2$	5.6	$149^\circ$
7	$9.2 \pm 1.9$	4.4	$167^\circ$
8	$9.8 \pm 1.8$	4.7	$156^\circ$
9	$9.5 \pm 1.8$	4.6	$162^\circ$
10	$5.8 \pm 1.5$	2.8	$149^\circ$

<sup>a</sup> GPS monument positions and reference numbers are shown in Fig. 3.

<sup>b</sup> Mean horizontal displacement was calculated as the difference between the mean positions measured on 10 December 2004 and positions measured on 9 January 2007. GPS monument position errors are expressed as  $x$ -,  $y$ - and  $z$ -axis errors that define a 95% confidence ellipsoid. Displacement errors were calculated with these 95% confidence ellipsoids. We only report horizontal displacements because vertical displacements were usually within error.

<sup>c</sup> Displacement rates are calculated by dividing the mean displacement distance by the measurement period of 25 months.

<sup>d</sup> Displacement direction is expressed as an azimuth angle, clockwise from North ( $0^\circ$ ).

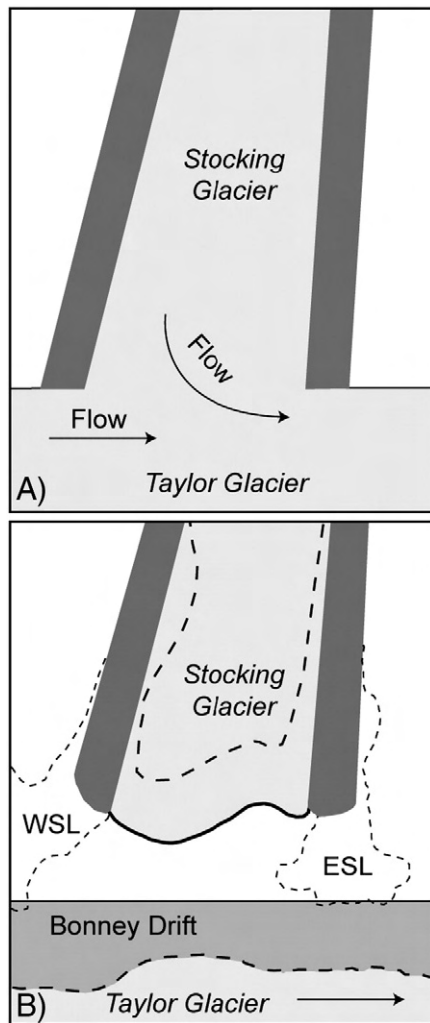


**Fig. 9.** Schematic diagram illustrating two possible origins for the distribution of ice-cored moraines in association with Stocking Glacier. In (A), the lack of a terminal, ice-cored moraine loop circumscribing Stocking Glacier arises because stocking ice merges with, and feeds, an expanded Taylor Glacier (e.g., Bockheim et al., 2008). In (B), the advance of Stocking Glacier is limited and there is no physical connection with an expanded Taylor Glacier. In this case, the lack of an ice-cored terminal moraine loop arises from the localized distribution of rockfall onto Stocking Glacier (see text). The dotted outlines indicate the current configuration of Stocking and Taylor Glaciers and the movement of the ESL and its western counterpart, West Stocking Lobe (WSL), to their current positions. We favor option (B) because the mapped upper limit of Taylor Glacier during its last major advance (MIS 5; Bonney drift in Fig. 2) lies well below the outermost drop moraine from Stocking Glacier, also tentatively correlated with MIS 5 glaciation (Higgins et al., 2000). Hence, during its latest advance, Stocking Glacier did not merge with Taylor Glacier (see also Denton et al., 1989).

at the survey site for minimal subsurface-ice flow. Therefore, to a first order, the modeling results are consistent with a core of relatively clean ice throughout most, if not all, of the ESL.

### 3.3. Using modern horizontal ice velocities to estimate the age of ice in the ESL

The outermost drop moraine (mapped in Figs. 2 and 3) is located ~400 m beyond the modern snout of Stocking Glacier (see also Higgins et al., 2000). If we assume that the ESL formed when Stocking Glacier reached this outermost position (and extended no further than this position) and that it subsequently flowed to its current terminus (~200 m lower in elevation and ~600 m downslope) at an average rate of  $\sim 4.5 \text{ mm a}^{-1}$  (the average rate during the study interval), then we can calculate an approximate age for the ice in the ESL (~600 m of displacement at  $4.5 \text{ mm a}^{-1}$ ). Doing so yields an age of  $\sim 130,000$  yrs.

This age is in accord with estimates for the last major expansion of alpine glaciers in Taylor Valley ( $\sim 115,000$ – $130,000$  years ago; Denton et al., 1989; Brook et al., 1993; Denton and Marchant, 2000; Higgins et al., 2000). We recognize that flow rates likely varied over time due to climate and topographic effects, but the first-order treatment is sufficient for our broad conclusion that ice in the ESL most likely dates to the last global interglacial, marine oxygen isotope stage 5.

### 3.4. Ice preservation as a function of microclimate zone and implications for long-term climate change in the MDV

Excess ice occurs within all three microclimate zones of the MDV (Hassinger and Mayewski, 1983; Denton and Marchant, 2000; Marchant et al., 2002). In the coastal thaw zone, buried, remnant glacier ice associated with the late Wisconsinan Ross Sea glaciation (Denton and Hughes, 1981; Denton and Marchant, 2000; Hall and Denton, 2000; Pollard et al., 2002) shows extensive evidence for degradation by thermokarst and active-layer cryoturbation (Denton and Marchant, 2000; Swanger and Marchant, 2007) (Fig. 10A). In the inland mixed zone examined here, excess ice in the ESL experiences some melting, but evidence for this comes from isotopic changes rather than from widespread thermokarst and/or other melt-related changes in ice-surface morphology (Fig. 10B). In the stable upland zone, multi-million-year-old buried glacier ice still retains its original isotopic signature, and overlying debris shows no evidence for transport by meltwater (Marchant et al., 2002; Souchez and Lorrain, 2006). For example, debris that caps Mullins Glacier in upper Beacon Valley (Figs. 1 and 10C), contains clasts that still retain percussion marks and fringing rock powder associated with ancient rock fall onto glacier ice (Marchant et al., 2007).

The contrast between pristine drift in Mullins Valley and the stratified drift on the ESL is striking (Fig. 10), even though both occur within the confines of a hyper-arid, cold-polar desert and mean annual air temperatures between the two sites differ by  $<2^\circ\text{C}$  (as measured during 2004 and 2006) (Table 1). An important point that follows from this comparison is that, in polar deserts, microclimatic variations play a major role in regulating the abundance of liquid meltwater and in controlling the rate and style of modification/preservation of shallow buried ice (Marchant and Head, 2007). Taking this point one step further, it is reasonable to infer that summertime environmental conditions along Mullins Glacier have not reached the relatively warm conditions now found at the ESL (e.g., in 2006 mean summertime temperatures were  $\sim 5^\circ\text{C}$  warmer at the ESL than at Mullins Glacier). Had such summer warming occurred, especially if prolonged over hundreds to thousands of years, we would predict that drift on Mullins Glacier (if not all eroded) would show stratigraphic evidence for ephemeral stream channels and fans, such as bedded sands, and that near-surface ice would have an isotopic signature consistent with melting and refreezing (as at the ESL); none of which, however, is the case (Marchant et al., 2002, 2007; Souchez and Lorrain, 2006). The purported age for distal regions of Mullins Glacier is  $\sim 7.9$  Myr (Marchant et al., 2007). If we assume that this age is valid and that evidence for cryoturbation and water reworking would be preserved in the stratigraphic record, then the combined results suggest that for the last  $\sim 7.9$  Myr the average summertime atmospheric temperatures in Mullins Valley have not increased by more than  $\sim 5^\circ\text{C}$  above present values for an extended period of time (e.g., the difference in mean December atmospheric temperature at the Stocking and Mullins glaciers; Table 1). This assertion is consistent with the notion of enduring, extremely cold and hyper-arid conditions at high elevations in the MDV since at least mid- to late-Miocene time (Marchant et al., 1993, 1996; Lewis et al., 2007).

## 4. Conclusions

We examined the age and origin of the East Stocking Lobe, a viscous flow lobe in central Taylor Valley. On the basis of integrated

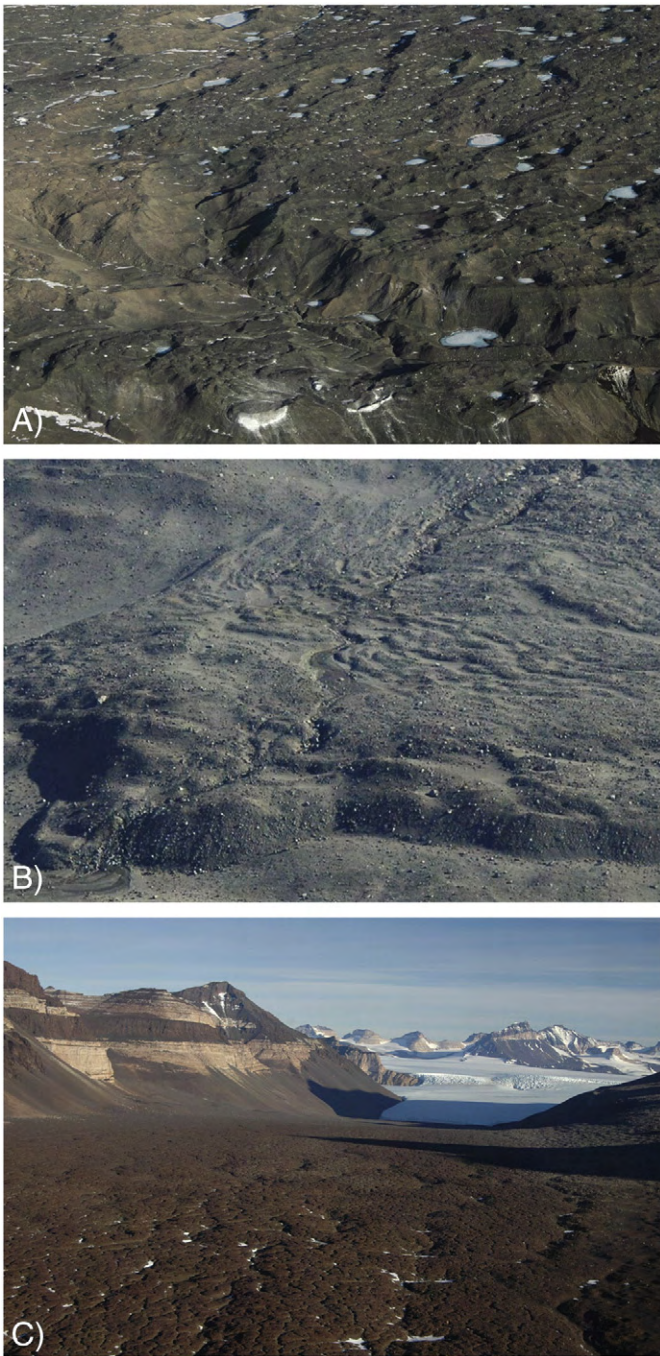


**Fig. 10.** Variable morphologies for buried ice in the McMurdo Dry Valleys as a function of microclimate zone. (A) Widespread thermokarst degradation of late Wisconsinan-age, buried glacier ice in the coastal thaw zone, ~1 km from the Ross Sea coast and ~120 m elevation. Circular depressions are filled with ponds that thaw during peak summer conditions (Denton and Marchant, 2000); field of view in foreground is ~500 m. (B) ESL in the inland mixed zone, ~40 km from the coast and ~600-m elevation. Our stable isotopic data from buried ice indicate periods of melting and refreezing, coupled with evaporation and/or sublimation. Morphologic change associated with widespread thermokarst is lacking, and active meltwater is not pervasive, but is instead localized alongside melting snow banks and melting streams; field of view in foreground is ~300 m. (C) Debris-covered glacier ice in the stable upland zone, [distal Mullins Glacier in the foreground, and buried Miocene-age ice in background (the latter is described in Sugden et al., 1995 and Marchant et al., 2002)], ~80 km from the coast and ~1300 m elevation. The surface debris on Mullins Glacier is ~50 to 70 cm thick, dry, and marked by sublimation polygons (e.g., Levy et al., 2006). Buried ice retains its primary (meteoric) isotopic composition (e.g., Sugden et al., 1995; Souchez and Lorrain, 2006), indicating that it has not been modified by extensive melting and refreezing; field of view in foreground is ~600 m. Altogether, the data show a progressive increase in the degradation of buried-ice deposits from the high-elevation stable upland zone, to the inland mixed zone, and finally to the coastal thaw zone.

field mapping, shallow seismic surveys, geospatial measurements, isotopic analyses, and numerical flow modeling, our results are most consistent with an origin for the East Stoking Lobe as an ice-cored moraine formed alongside the Stoking Glacier ~130 ka and modified by subsequent downslope flow at an average rate of 4 to 5 mm a<sup>-1</sup>. Today the lobe contains buried glacier ice as much as 14 to 30 m thick; the uppermost 30 cm of which, at least, has been modified by freeze/thaw processes and sublimation and/or evaporation. This modification is inferred from low deuterium excess values, and from  $\delta D$  vs.  $\delta^{18}O$  data that plot on a slope of 5.8, well below the local meteoric water line. Since deposition, the ice-cored moraine has flowed downslope ~600 m.

The drift that caps the ESL shows extensive morphological and sedimentological evidence for transport by liquid water. This extensive reworking is in marked contrast with relatively pristine drift, unmarked by liquid water, that caps buried glacier ice at higher elevations within the stable upland zone of the MDV (Marchant et al., 2002, 2007; Kowalewski et al., 2006; Marchant and Head, 2007). Our comparison of the two drift types, and of the local environmental conditions at each site, implies that summertime atmospheric temperatures at the Mullins Glacier have likely remained below ~-4 °C (the mean summertime conditions at the ESL) for the last several million years (perhaps the last 7+ million years).

Finally, we show that the spatial distribution of ice-cored moraines and ice-cored drift, such as the ESL, appears closely related to the location of rockfall from suitable bedrock cliffs. Where rockfall is abundant, ice-cored moraines typically form, and where absent or relatively minor, drop moraines are likely the norm. In regions where ice-cored lobes occur in isolation and are not linked with active glacier ice, the lobes may be one of the few geomorphic features to signify the general location of former alpine glaciers.

## Acknowledgements

We thank David Shean for excellent assistance in the field and for insight regarding seismic and GPS data. We also thank Thomas Nylen of UNAVCO for help in acquiring and processing the high-resolution GPS measurements, and Robert Michener who analyzed the stable isotopes. Finally, we thank two anonymous reviewers whose comments helped improve this manuscript greatly. Funding for this research was provided by NSF Polar Programs Grant ANT-0636705 and NASA Mars Fundamental Research Program Grant NNX-06AE32G to DRM.

## References

- Ackert Jr., R.P., 1998. A rock glacier/debris-covered glacier system at Galena Creek, Absaroka Mountains, Wyoming. *Geografiska Annaler* 80A (3–4), 267–276.
- Allard, M., Caron, S., Begin, Y., 1996. Climatic and ecological controls on ice segregation and thermokarst: the case history of a permafrost plateau in northern Quebec. *Permafrost and Periglacial Processes* 7, 207–227.
- Allibone, A., Wysoczanski, R., 2002. Initiation of magmatism during the Cambrian–Ordovician Ross orogeny in southern Victoria Land, Antarctica. *Geological Society of America Bulletin* 114, 1007–1018.
- Atkins, C.B., Dickinson, W.W., 2007. Landscape modification by meltwater channels at margins of cold-based glacier, Dry Valleys, Antarctica. *Boreas* 36, 47–55.
- Balco, G., Shuster, D.L., 2009. Production rate of cosmogenic <sup>21</sup>Ne in quartz estimated from <sup>10</sup>Be, <sup>26</sup>Al, and <sup>21</sup>Ne concentration in slowly eroding Antarctic bedrock surfaces. *Earth and Planetary Science Letters* 281, 48–58.
- Barrett, P.J., 1981. History of the Ross Sea region during the deposition of the Beacon Supergroup 400 to 180 million years ago. *Journal of the Royal Society of New Zealand* 11, 447–458.
- Bennett, M.R., Huddart, D., Glasser, N.F., Hambrey, M.J., 2000. Resedimentation of debris on an ice-cored lateral moraine in the high-Arctic (Kongsvegen, Svalbard). *Geomorphology* 35, 21–40.
- Berg, T.E., Black, R.F., 1966. Preliminary measurements of growth of non-sorted polygons, Victoria Land, Antarctica. *American Geophysical Union Antarctic Research Series* 8, Washington, CD, USA, pp. 61–108.
- Bockheim, J.G., Prentice, M.L., McLeod, M., 2008. Distribution of glacial deposits, soils, and permafrost in Taylor Valley, Antarctica. *Arctic, Antarctic, and Alpine Research* 40 (2), 279–286.
- Brook, E.J., Kurz, M.D., Ackert Jr., R.P., Denton, G.H., Brown, E.T., Raisbeck, G.M., Yiou, F., 1993. Chronology of Taylor Glacier Advance in Arena Valley, Antarctica, using in situ cosmogenic <sup>3</sup>He and <sup>10</sup>Be. *Quaternary Research* 39, 11–23.

- Cardyn, R., Clark, I.D., Lacelle, D., Lauriol, B., Zdanowicz, C., Calmels, F., 2007. Molar gas ratios entrapped in ice: a new tool to determine the origin of relict massive ground ice bodies in permafrost. *Quaternary Research* 68, 239–248.
- Cheng, G., 1983. The mechanism of repeated-segregation for the formation of thick layered ground ice. *Cold Regions Science and Technology* 8, 57–66.
- Clark, D.H., Steig, E.J., Potter Jr., N., Gillespie, A.R., 1998. Genetic variability of rock glaciers. *Geografiska Annaler* 80 (3/4), 175–182.
- Craig, H., 1961. Isotopic variations in meteoric waters. *Science* 133, 1702–1703.
- Cuffey, K.M., Conway, H., Gades, A.M., Hallet, B., Lorrain, R., Severinghaus, J.P., Steig, E.J., Vaughn, B., White, J.W.C., 2000. Entrainment at cold glacier beds. *Geology* 28 (4), 351–354.
- Dansgaard, W., 1964. Stable isotopes in precipitation. *Tellus* 16, 436–468.
- Denton, G.H., Hughes, T.J., 1981. *The Last Great Ice Sheets*. Wiley, Chichester, United Kingdom. 484 pp.
- Denton, G.H., Marchant, D.R., 2000. The geologic basis for a reconstruction of a grounded ice sheet in McMurdo Sound, Antarctica, at the last glacial maximum. *Geografiska Annaler* 82A, 167–211.
- Denton, G.H., Bockheim, J.G., Wilson, S.C., Stuiver, M., 1989. Late Wisconsin and early Holocene glacial history, inner Ross Embayment, Antarctica. *Quaternary Research* 31, 151–182.
- Doran, P.T., McKay, C.P., Clow, G.D., Dana, G.L., Fountain, A.G., Nysten, T., Lyons, W.B., 2002. Valley floor climate observations from the McMurdo dry valleys, Antarctica, 1986–2000. *Journal Geophysical Research* 107, D244772. doi:10.1029/2001JD002045.
- Elliot, D.H., Fleming, T.H., 2004. Occurrence and dispersal of magmas in the Jurassic Ferrar Large Igneous Province, Antarctica. *Gondwana Research* 7, 223–237.
- Fountain, A.G., Lewis, K.J., Doran, P.T., 1999. Spatial climatic variation and its control on glacier equilibrium line altitude in Taylor Valley, Antarctica. *Global and Planetary Change* 22, 1–10.
- Fountain, A.G., Nysten, T.H., Monaghan, A., Basagic, H.J., Bromwich, D., 2009. Snow in the McMurdo Dry Valleys, Antarctica. *International Journal of Climatology*. doi:10.1002/joc.1933.
- Giacomini, F., Tiepolo, M., Dallai, L., Ghezzi, C., 2007. On the onset and evolution of the Ross-orogeny magmatism in North Victoria Land—Antarctica. *Chemical Geology* 240, 103–128.
- Gillies, J.A., Nickling, W.G., Tilson, M., 2009. Ventifacts and wind-abraded rock features in the Taylor Valley, Antarctica. *Geomorphology* 107 (3–4), 149–160.
- Gooseff, M.N., Lyons, W.B., McKnight, D.M., Vaughn, B.H., Fountain, A.G., Dowling, C., 2006. A stable isotopic investigation of a polar desert hydrologic system, McMurdo Dry Valleys, Antarctica. *Arctic, Antarctic, and Alpine Research* 38 (1), 60–71.
- Hall, B.L., Denton, G.H., 2000. Radiocarbon chronology of Ross Sea drift, eastern Taylor Valley, Antarctica; evidence for a grounded ice sheet in the Ross Sea at the last glacial maximum. *Geografiska Annaler* 82A, 305–336.
- Hassinger, J.M., Mayewski, P.A., 1983. Morphology and dynamics of the rock glaciers in southern Victoria Land, Antarctica. *Arctic and Alpine Research* 15 (3), 351–368.
- Head, J.W., Marchant, D.R., Dickson, J., Levy, J., Morgan, G., 2007. Transient streams and gullies in the Antarctic Dry Valleys: geological setting, processes and analogs to Mars. In Cooper, A.K., Barrett, P.J., Stagg, H., Storey, B., Stump, E., Wise, W., and the 10th ISAES editorial team (Eds.), *Antarctica: A Keystone in a Changing World—Online Proceedings of the 10th ISAES*, edited by A.K. Cooper and C.R. Raymond et al., USGS Open-File Report 2007-1047, Extended Abstract 151, 4 pp.
- Higgins, S.M., Hendy, C.H., Denton, G.H., 2000. Geochronology of Bonney Drift, Taylor Valley, Antarctica: evidence for interglacial expansions of Taylor Glacier. *Geografiska Annaler* 82A, 391–409.
- Humlum, O., 1998. The climatic significance of rock glaciers. *Permafrost and Periglacial Processes* 9, 375–395.
- Kaab, A., Weber, M., 2004. Development of transverse ridges on rock glaciers: field measurements and laboratory experiments. *Permafrost and Periglacial Processes* 15, 379–391.
- Konrad, J.-M., 2005. Estimation of the segregation potential of fine-grained soils using the frost heave response of two reference soils. *Canadian Geotechnical Journal* 42, 38–50.
- Konrad, S.K., Humphrey, N.F., Steig, E.J., Clark, D.H., Potter, N., Pfeffer, W.T., 1999. Rock glacier dynamics and paleoclimatic implications. *Geology* 27 (12), 1131–1134.
- Kowalewski, D.E., Marchant, D.R., Levy, J.S., Head III, J.W., 2006. Quantifying summertime sublimation rates for buried glacier ice in Beacon Valleys, Antarctica. *Antarctic Science* 18, 421–428.
- Lacelle, D., Lauriol, B., Clark, I.D., Cardyn, R., Zdanowicz, C., 2007. Nature and origin of a Pleistocene-age massive ground-ice body exposed in the Chapman Lake moraine complex, central Yukon Territory, Canada. *Quaternary Research* 68, 249–260.
- Lacelle, D., St-Jean, M., Lauriol, B., Clark, I.D., Lewkowicz, A., Froese, D.G., Kuehn, S.C., Zazula, G., 2009. Burial and preservation of 30,000 year old perennial snowbank in Red Creek valley, Ogilvie Mountains, central Yukon, Canada. *Quaternary Science Reviews* 28, 3401–3413.
- Lawson, D.E., 1983. Ground ice in perennially frozen sediments, northern Alaska. *Proceedings, Fourth International Conference on Permafrost*. National Academy Press, Washington, DC, USA, pp. 695–700.
- Levy, J.S., Marchant, D.R., Head III, J.W., 2006. Distribution and origin of patterned ground on Mullins Valley debris-covered glacier, Antarctica: the roles of ice flow and sublimation. *Antarctic Science* 18, 385–397.
- Levy, J.S., Head III, J.W., Marchant, D.R., 2008. The role of thermal contraction crack polygons in cold-desert fluvial systems. *Antarctic Science*. doi:10.1017/S0954102008001375.
- Lewis, A.R., Marchant, D.R., Ashworth, A.C., Hemming, S.R., Machlus, M.L., 2007. Major middle Miocene global climate change; evidence from East Antarctica and the Transantarctic Mountains. *Geological Society of America Bulletin* 119 (11–12), 1449–1461.
- Liboutry, L., 1966. *Traite de Glaciologie*, vol. 2. Masson, Paris.
- Mackay, J.R., 1972. The world of underground ice. *Annals Association of American Geographers* 62, 1–22.
- Mackay, J.R., Dallimore, S.R., 1992. Massive ice of the Tuktoyaktuk area, western Arctic coast, Canada. *Canadian Journal of Earth Science* 29, 1235–1249.
- Marchant, D.R., Denton, G.H., 1996. Miocene and Pliocene paleoclimate of the Dry Valleys region, southern Victoria Land: a geomorphological approach. *Marine Micropalaeontology* 27, 253–271.
- Marchant, D.R., Head III, J.W., 2007. Antarctic dry valleys: microclimate zonation, variable geomorphic processes, and implications for assessing climate change on Mars. *Icarus* 192, 187–222.
- Marchant, D.R., Denton, G.H., Swisher III, C.C., 1993. Miocene–Pliocene–Pleistocene glacial history of Arena Valley, Quartermain Mountains, Antarctica. *Geografiska Annaler* 75A, 269–302.
- Marchant, D.R., Denton, G.H., Swisher III, C.C., Potter Jr., N., 1996. Late Cenozoic Antarctic paleoclimate reconstruction from volcanic ashes in the Dry Valleys region of southern Victoria Land. *Geological Society of America Bulletin* 108, 181–194.
- Marchant, D.R., Lewis, A.R., Phillips, W.M., Moore, E.J., Souchez, R.A., Denton, G.H., Sugden, D.E., Potter Jr., N., Landis, G.P., 2002. Formations of patterned ground and sublimation till over Miocene glacier ice in Beacon Valley, southern Victoria Land, Antarctica. *Geological Society of America Bulletin* 114, 718–730.
- Marchant, D.R., Phillips, W.M., Schaefer, J.M., Winckler, G., Fastook, J.L., Shean, D.E., Kowalewski, D.E., Head III, J.W., Lewis, A.R., 2007. Establishing a chronology for the world's oldest glacier ice. In Cooper, A.K., Barrett, P.J., Stagg, H., Storey, B., Stump, E., Wise, W., and the 10th ISAES editorial team (Eds.), *Antarctica: A Keystone in a Changing World—Online Proceedings of the 10th ISAES*, edited by A.K. Cooper and C.R. Raymond et al., USGS Open-File Report 2007-1047, Extended Abstract 054, 4p.
- Moorman, B.J., Michel, F.A., 2000. The burial of ice in the proglacial environment on Bylot Island, Arctic Island. *Permafrost and Periglacial Processes* 11, 161–175.
- Nichols, R.L., 1968. Coastal geomorphology, McMurdo Sound, Antarctica. *Journal of Glaciology* 7, 449–478.
- Northcutt, M.L., Gooseff, M.N., Barrett, J.E., Zeglin, L.H., Takacs-Vesbach, C.D., Humphrey, J., 2009. Hydrologic characteristics of lake- and stream-side riparian wetted margins in the McMurdo Dry Valleys, Antarctica. *Hydrological Processes* 23 (9), 1255–1267.
- Osterkamp, T.E., Romanovsky, V.E., 1999. Evidence for warming and thawing of discontinuous permafrost in Alaska. *Permafrost and Periglacial Processes* 10, 17–37.
- Paterson, W.S.B., 1994. *The Physics of Glaciers*, 3rd Edition. Pergamon, Elsevier Science Ltd., Oxford, United Kingdom.
- Petit, J.R., Jouzel, J., Raynaud, D., Barkov, N.I., Barnola, J.M., Basile, I., Bender, M., Chappellaz, J., Davis, M., Delmotte, G., Delmotte, M., Kotlyakov, V.M., Legrand, M., Lipenkov, V.Y., Lorius, C., Pepin, L., Ritz, C., Saltzman, E., Stievenard, M., 1999. Climate and atmospheric history of the past 420,000 years from the Vostok ice core, Antarctica. *Nature* 399, 429–436.
- Pollard, W., Doran, P., Wharton, R., 2002. The nature and significance of massive ground ice in Ross Sea Drift, Garwood Valley, McMurdo Sound, Royal Society of New Zealand Bulletin, 35 (Antarctica at the Close of the Millennium), pp. 397–404.
- Schaefer, J.M., Baur, H., Denton, G.H., Ivy-Ochs, S., Marchant, D.R., Schluchter, C., Weisler, R., 2000. The oldest ice on Earth in Beacon Valley, Antarctica: new evidence from surface exposure dating. *Earth and Planetary Science Letters* 179, 91–99.
- Schorghofer, 2005. A physical mechanism for long-term survival of ground ice in Beacon Valley, Antarctica. *Geophysical Research Letters* 32, L19503. doi:10.1029/2005GL023881.
- Serrano, E., Lopez-Martinez, J., 2000. Rock glaciers in the South Shetland Islands, western Antarctica. *Geomorphology* 35, 145–162.
- Shean, D.E., Marchant, D.R., 2010. Seismic and GPR surveys of Mullins Glacier, McMurdo Dry Valleys, Antarctica: ice thickness, internal structure and implications for surface ridge formation. *Journal of Glaciology* 56 (195), 48–64.
- Shean, D.E., Head III, J.W., Marchant, D.R., 2007. Shallow seismic surveys and ice thickness estimates of the Mullins Valley debris-covered glacier, McMurdo Dry Valleys, Antarctica. *Antarctic Science* 19 (4), 485–496.
- Souchez, R., Lorrain, R., 2006. The environmental significance of deuterium excess in meteoric and non-meteoritic Antarctic ice. In: Knight, P. (Ed.), *Glacier Science and Environmental Change*. Blackwell Pub., Oxford, United Kingdom, pp. 179–184.
- Steig, E.J., Clark, D.H., Potter Jr., N., Gillespie, A.R., 1998a. The geomorphic and climatic significance of rock glaciers. *Geografiska Annaler* 80A, 173–174.
- Steig, E.J., Fitzpatrick, J.J., Potter Jr., N., Clark, D.H., 1998b. The geochemical record in rock glaciers. *Geografiska Annaler* 80A, 277–286.
- Stockwell, J.W., 1999. The CWP/SU: seismic Un\*x package. *Computers and Geosciences* 25, 415–419.
- Sugden, D.E., Marchant, D.R., Potter Jr., N., Souchez, R.A., Denton, G.H., Swisher III, C.C., Tison, J.-L., 1995. Preservation of Miocene glacier ice in East Antarctica. *Nature* 376, 412–414.
- Summerfield, M.A., Stuart, F.M., Cockburn, H.A.P., Sugden, D.E., Dunai, T., Marchant, D.R., 1999. Long-term rates of denudation in the Dry Valleys, Transantarctic Mountains, southern Victoria Land, Antarctica based on in-situ-produced cosmogenic <sup>21</sup>Ne. *Geomorphology* 27, 113–129.
- Swanger, K.M., Marchant, D.R., 2007. Sensitivity of ice-cemented Antarctic soils to greenhouse-induced thawing: are terrestrial archives at risk? *Earth and Planetary Science Letters* 259, 347–359.
- Whalley, W.B., Martin, H.E., 1992. Rock glaciers: II. Models and mechanisms. *Progress in Physical Geography* 16 (2), 127–186.